

Determining the optimal focusing parameter in sparse promoting inversions of EMI surveys

Wouter Deleersnyder ^{a,b*}; David Dudal ^{a,c†}; Benjamin Maveau ^{a‡}; Marieke Paepen ^{b§}

^a *KU Leuven Campus Kortrijk – Kulak, Department of Physics, Etienne Sabbelaan 53 bus 7657, 8500 Kortrijk, Belgium*

^b *Ghent University, Department of Geology, Krijgslaan 281-S8, 9000 Gent, Belgium*

^c *Ghent University, Department of Physics and Astronomy, Krijgslaan 281-S9, 9000 Gent, Belgium*

Abstract

If the magnetic field caused by a magnetic dipole is measured, the electrical conductivity of the subsurface can be determined by solving the inverse problem. For this problem a form of regularisation is required as the forward model is badly conditioned. Commonly, Tikhonov regularisation is used which adds the ℓ_2 -norm of the model parameters to the objective function. As a result, a smooth conductivity profile is preferred and these types of inversions are very stable. However, it can cause problems when the true profile has discontinuities causing oscillations in the obtained model parameters. To circumvent this problem, ℓ_0 -approximating norms can be used to allow discontinuous model parameters. Two of these norms are considered in this paper, the Minimum Gradient Support and the Cauchy norm. However, both norms contain a parameter which transforms the function from the ℓ_2 - to the ℓ_0 -norm. To find the optimal value of this parameter, a new method is suggested. It is based on the L -curve method and finds a good balance between a continuous and discontinuous profile. The method is tested on synthetic data and is able to produce a conductivity profile similar to the true profile. Furthermore, the strategy is applied to newly acquired real-life measurements and the obtained profiles are in agreement with the results of other surveys at the same location. Finally, despite the fact that the Cauchy norm is only occasionally used to the best of our knowledge, we find that it performs at least as good as the Minimum Gradient Support norm.

1 Introduction

Frequency domain electromagnetic induction (FDEM) uses a coil with an alternating current as a source while, at a distance, a second coil measures the magnetic response. This magnetic field allows one to estimate the electrical conductivity profile of the soil, albeit that the reconstructed conductivity is not unique in general. The profile can be used to monitor

*wouter.deleersnyder@kuleuven.be

†david.dudal@kuleuven.be

‡benjamin.maveau@kuleuven.be (corresponding author)

§marieke.paepen@ugent.be

chemical pollution (Martinelli and Duplaá, 2008; Deidda et al., 2022), search for archeological structures (Saey et al., 2012) or detect saltwater intrusion (Scudiero et al., 2011). All of this is done in a non-destructive way and, because it is a non-contacting method, measurements are done rather easily.

To transform the measurements (i.e. the magnetic field) to a conductivity profile, we need to solve the so called inverse problem which, in essence, is an optimization problem. The objective function that needs to be minimised contains the misfit between the measured data and the data generated from the model parameters, the conductivity profile in our case. This optimisation is highly unstable creating solutions which are strongly dependent on the measurement error. Moreover, the solution is hardly unique. We therefore use a process called regularisation which alters our objective function to prefer geophysical probable solutions. Tikhonov regularisation (Tikhonov, 1943) is frequently used, leading to a smooth conductivity profile.

However, there are multiple reasons why a piecewise continuous profile is more appropriate. The number of data points in electromagnetic induction (EMI) surveys are small, reducing the resolution and making it less sensitive to a rapid change in conductivity. A piecewise continuous profile allows a large change in conductivity. Combining this with a fine resolution in the inverted profile, we can give a good estimate on the location of the interface. For smooth profiles on the contrary, the profile will show a transition zone between layers and the interface depth will be subject to interpretation. Different methods exist to abandon smooth model parameters (Farquharson, 2007; Paasche and Tronicke, 2007; Hermans et al., 2012; Deleersnyder et al., 2021; Thibaut et al., 2021) but they either require prior knowledge or fixing (a) parameter(s) in the inversion. As the ℓ_2 -norm causes oscillations at discontinuities (Farquharson and Oldenburg, 1998; Loke et al., 2003), most of the previous mentioned methods abandon this norm in favour of the ℓ_0 - and ℓ_1 -norm¹. These are much more suited for the desired model parameters, but these norms are not continuous. Several, continuous, approximations to these norms exist such as the Minimum Support (Last and Kubik, 1983) or the Cauchy log norm (Guitton, 2012), see Equations 5-6. All of these depend on a parameter, which we call the focusing parameter and interpolates the norm between ℓ_2 and ℓ_0 .

The importance of this parameter was already established in (Blaschek et al., 2008): a too small value causes small changes in conductivity to be ignored while a too large value will cause oscillations at discontinuities. In this paper, we therefore suggest a new method to determine this parameter, based on a scheme similar to the L -curve method. We first discuss our inversion method. We then apply our method on three synthetic conductivity profiles. The first one is a simple three layer soil profile and we use a smoothed version as the second profile. The third synthetic profile is generated from the conductivity profile obtained from borehole logging at Hermalle-sous-Argenteau (Belgium) along the river Meuse. Finally we apply it on data collected at De Westhoek, a nature reserve in De Panne (Belgium). At this site, saltwater intrusion causes a sharp conductivity spike in the profile, which we are effectively able to locate with our new method.

¹Most often, the ℓ_0 -norm of a vector $\mathbf{x} = (x_1, \dots, x_n)$ is seen as the number of non-zero elements x_i . This definition, however, does not obey all the mathematical requirements of a proper norm. For completeness, we recall that in general, for $p \geq 1$, the ℓ_p -norm of \mathbf{x} is defined via $\|\mathbf{x}\|_p = (|x_1|^p + \dots + |x_n|^p)^{1/p}$.

2 Inversion method

Our inverse problem consists of minimising the objective function

$$\phi(\mathbf{m}) = \phi_d\left(\frac{1}{m}W_d \cdot (\mathbf{F} - \mathbf{d})\right) + \lambda\phi_m(W_m \cdot \log(\mathbf{m})), \quad (1)$$

where ϕ_d is the ℓ_2 norm function, $W_{d,m}$ are reweighing matrices, \mathbf{F} is the forward model, \mathbf{d} is the data of size m and ϕ_m is the regularisation function. The latter is necessary due to the difference $\boldsymbol{\eta}$ between the exact and the measured data, and the non-linearity of the forward model. For the latter, we use the damped model, which is a recently developed quasi-linear model with only a slight error w.r.t. the exact analytical solution (Delrue et al., 2020) on condition that the induction number is small enough i.e. $\mu\omega\sigma s^2 \ll 1$. We set W_d equal to $\text{diag}(\boldsymbol{\eta}^{-1})$ and choose λ so that ϕ_d is slightly larger than 1. This is based on the discrepancy principle (Morozov, 1966), stating that the mismatch between \mathbf{F} and \mathbf{d} must be equal or larger than the error $\boldsymbol{\eta}$ on the data. Finally, the matrix W_m can be any matrix, but is commonly the identity matrix or a matrix implementing a discretization of the derivative.

We solve this optimization problem using the Gauss-Newton algorithm, which requires the derivative

$$\nabla_{\mathbf{m}}\phi(\mathbf{m}) = J^\dagger \cdot \Psi \cdot \mathbf{r}, \quad (2)$$

where we defined the following symbols:

$$J = \begin{pmatrix} W_d G_F \\ \sqrt{\lambda} W_m \end{pmatrix}, \quad \mathbf{r} = \begin{pmatrix} W_d \mathbf{r}_d \\ \sqrt{\lambda} W_m \mathbf{m} \end{pmatrix}, \quad \Psi = \begin{pmatrix} \text{diag}\left(\frac{\phi'_d(W_d \cdot \mathbf{r}_d)}{W_d \cdot \mathbf{r}_d}\right) \\ \text{diag}\left(\frac{\phi'_m(W_m \cdot \mathbf{m})}{W_m \cdot \mathbf{m}}\right) \end{pmatrix}, \quad (3)$$

G_F is the gradient matrix of the forward function and ϕ'_x is the derivative of the norm function w.r.t. its argument. Taking the derivative of the gradient results in the Hessian $H[\phi(\mathbf{m})] = J^\dagger \cdot \Psi \cdot J$, where we neglected the second order derivatives. These have a small contribution as long as the residual \mathbf{r} is small (Nocedal and Wright, 2006), which should be the case if we are close enough to a minimum. To find a direction where the objective function is smaller, we evaluate it at $\mathbf{m} + \delta\mathbf{m}$, and use a Taylor expansion around \mathbf{m}

$$\phi(\mathbf{m} + \delta\mathbf{m}) = \phi(\mathbf{m}) + \nabla_{\mathbf{m}}\phi(\mathbf{m}) \cdot \delta\mathbf{m} + \delta\mathbf{m} \cdot H[\phi(\mathbf{m})] \cdot \delta\mathbf{m}.$$

The minimum of this function can readily be found if we neglect the third order in $\delta\mathbf{m}$. Indeed, we reduce our objective function to a quadratic equation in $\delta\mathbf{m}$, which minimum is equal to the solution of the following equation

$$(J^\dagger \cdot \Psi \cdot J) \cdot \delta\mathbf{m} = -\nabla\phi(\mathbf{m}). \quad (4)$$

To increase performance, we modify the algorithm in two ways. First, we demand a positive electrical conductivity, further reducing the model space. To accomplish this, we use the Gradient projection reduced Newton algorithm (Vogel, 2002)². Secondly, we also perform a line-search with the step determined from equation (4). Using the algorithm from

²By working in log space, one can also force the inversion towards a positive conductivity. We, however, noticed no improvement in speed or accuracy and we therefore used a bounded solver.

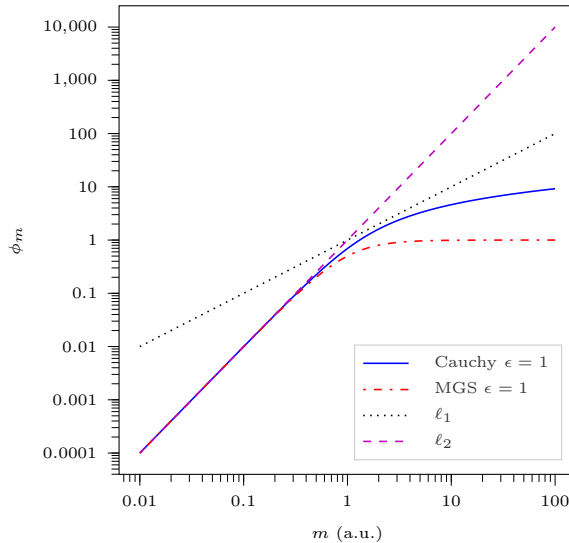


Figure 1: The different norms in function of the model parameters. The Cauchy and minimum gradient support (MGS) norm have a focusing parameter of 1.

(Moré and Thunten, 1994), we can assure that the first Wolfe condition is obeyed (Wolfe, 1969).

As already said, Tikhonov regularisation (Tikhonov, 1943) is probably the most common and simplest form of regularisation. It uses the ℓ_2 -norm as ϕ_m , resulting in smooth model parameters. Due to the nature of our problem, we, however, rather expect piecewise continuous model parameters. Mathematically, this translates in model parameters for which the differences between subsequent values are small apart from a few at the interfaces. Using the matrix

$$W_m = \begin{pmatrix} 1 & -1 & 0 & & & \\ 0 & 1 & -1 & & & \\ & & & \dots & & \\ & & & & 1 & -1 & 0 \\ & & & & 0 & 1 & -1 \end{pmatrix}$$

as reweighing matrix, we get a vector containing the differences between adjacent layers conductivities. This vector should be sparse to obtain a piecewise continuous conductivity profile. In this case an ℓ_0 -norm for ϕ_m is preferred.

Unfortunately, the derivative of the ℓ_0 -norm does not exist as the function is discontinuous. This is circumvented by using a smooth function which approximates the ℓ_0 -norm. While different approximating functions (e.g. Cauchy or Minimum (Gradient) Support—M(G)S³) exist, all depend on a focusing parameter ϵ . This focusing parameter balances between smooth

³Depending on the input of this function, it is either called the Minimum Gradient Support or the Minimum Support. The former takes the differences between conductivity layers as input (as in our case), while the latter uses the conductivity of the layers.

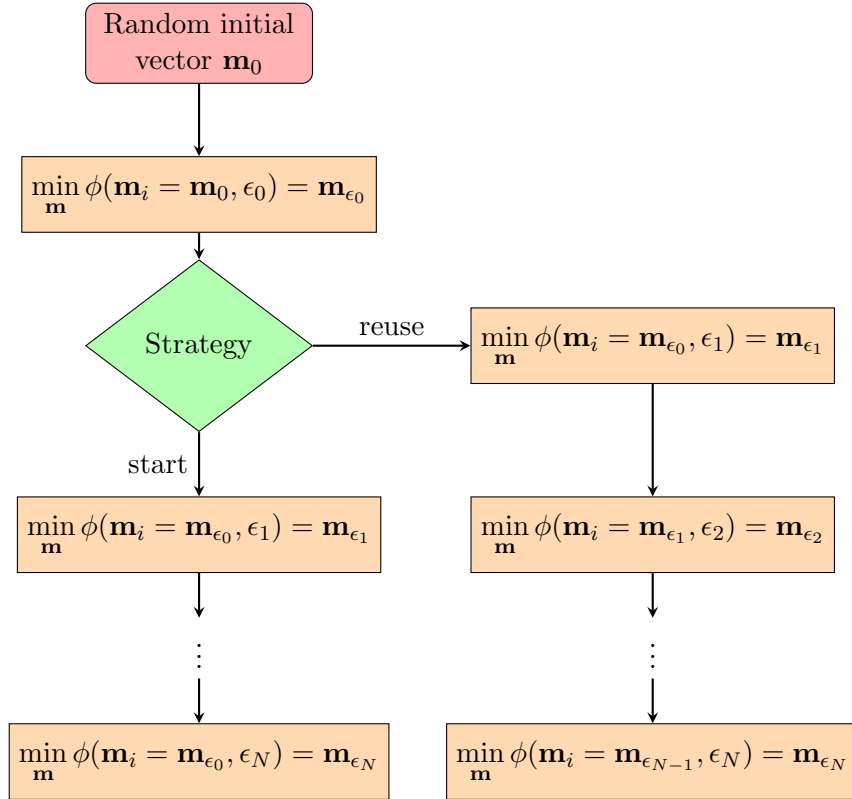


Figure 2: A flowchart to illustrate the start and reuse strategy. The argument \mathbf{m}_i of ϕ_m is the starting model parameter of the inversion. While the left branch (the start strategy) is shown sequentially, the subsequent inversions can be solved in parallel since they are independent on the previous solution.

and blocky model parameters and its importance cannot be overestimated. We used

$$\text{MGS:} \quad \phi_m(x) = \frac{x^2}{x^2 + \epsilon^2} \quad \text{and} \quad (5)$$

$$\text{Cauchy:} \quad \phi_m(x) = \ln\left(1 + \frac{x^2}{\epsilon^2}\right), \quad (6)$$

as both can get very blocky and smooth model parameters for small and large ϵ respectively. In Figure 1, these two norms are plotted in function of the model parameter together with the ℓ_1 - and ℓ_2 -norm. For small values of the model parameter with respect to the focusing parameter, the two behave similar to the ℓ_2 -norm. For larger values they diverge, but are both less-penalising than the ℓ_1 -norm. The Cauchy function keeps increasing for larger model parameters, albeit at a slower rate. The MGS, however, converges to the value of 1.

We will use the discrepancy principle to set the regularisation parameter λ but still need to determine the optimal focusing parameter ϵ . While a lot of literature exists on the selection of the former one, the latter is often set a priori. See Fiandaca et al. (2015) for a short overview of existing methods to determine this parameter. We will discuss a novel approach to find the optimal value of the focusing parameter.

Using our optimization algorithm described above, we solve the inverse problem for different

values of the focusing parameter. These values are uniformly chosen in log-space between 10^0 and 10^{-5} .

- We first solve the problem for the largest value of the focusing parameter, then we use this solution as starting point for all the other solvers. This prevents the problem of multimodality, which arises for smaller values of the focusing parameter. We call this the start strategy. As the method only requires the solution of the inversion with a large focusing parameter, we can easily compute the other results in parallel.
- Another approach uses the solution of the previous focusing parameter to get the next result. This method is called the reuse strategy. This causes a smoother and more stable L -curve, but it tends to flatten peaks in the conductivity profile. The latter is illustrated in the blocky 3-layer soil profile of Subsection 3.1.

Both strategies are illustrated in the flowchart of Figure 2. For every solution, we plot the data misfit in terms of the model misfit (see Figure 3). With the Cauchy norm, we get a J -shaped curve which has a jump in the data misfit on the horizontal line. This discontinuity happens when decreasing ϵ from 1.56×10^{-1} to 1.38×10^{-1} and changes the model parameters from smooth to blocky. Using the Cauchy norm, one can find two interesting results; a blocky result just after the discontinuity and a smooth result for a focusing parameter larger than the critical value 1.38×10^{-1} (see Figure 3). The smooth result is for both strategies the same, while the blocky model parameters can be very different.

In case of the MGS norm, the curve is different, especially for smaller ϵ . For larger ϵ , the model parameters are the same as with the Cauchy norm. The reuse method has two discontinuities, the first discontinuity changes the smooth profile to a smooth profile with one jump. The second discontinuity transforms the profile to a blocky one. With decreasing focusing parameters, the model parameters change only slightly. If we use the start strategy, three discontinuities appear. The first and last have the same effect as with the reuse strategy, while the second discontinuity changes the position of the jump in conductivity. Note that the start strategy produces blocky model parameters with a much larger data misfit.

In Figure 3 the regions of the different model parameters are plotted if the MGS norm is used. The two regions A and B, which both strategies have in common, produce a smooth and a semi-smooth result respectively. Both fail to find the conductivity of the third layer and the second interface depth. The semi-smooth result of region B, however, finds the first interface depth. With the start strategy, we get another semi-smooth region after the second discontinuity. The data misfit has increased significantly (from 1.2 to 1.6), and the model parameters have a smaller peak value than the results from region A and B. After the third discontinuity, the second one for the reuse strategy, we find the blocky region (denoted with D in the plot). This result shows the two interface depth clearly, with the reuse strategy finding almost the correct width (2.5 m) and height (700 mS m^{-1}). With the start strategy, the width (4 m) and height (500 mS m^{-1}) of the peak deviates more from the true values, again resulting in a much larger data misfit.

If we compare the L -curves, one may notice that the solvers using the Cauchy norm produce a more fluent shape than the curve generated from the solvers with the MGS norm. This can be understood from Figure 1. Indeed, the Cauchy norm penalises, albeit at a slower rate, an

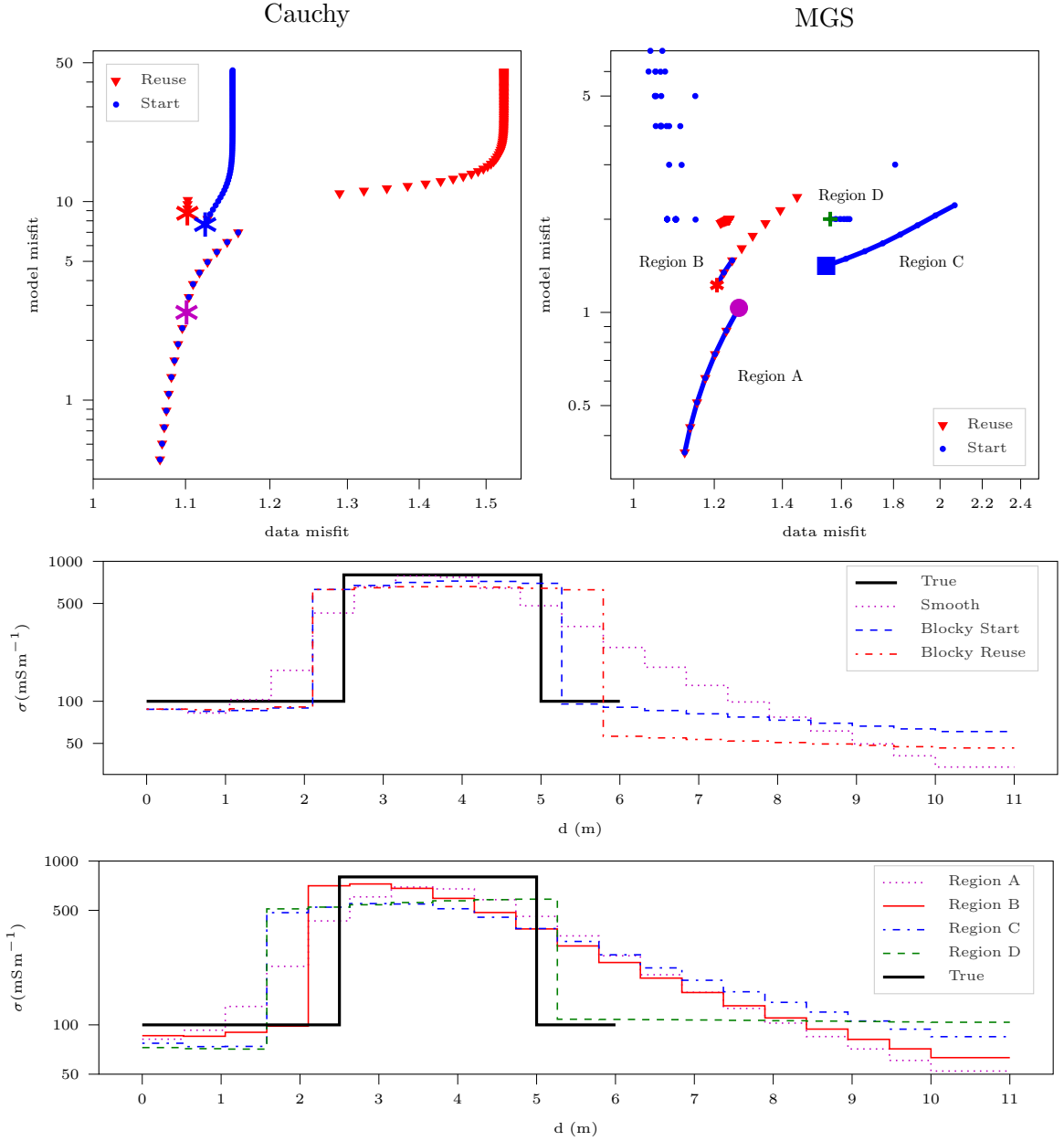


Figure 3: (top) The data and model misfit of the different solvers. The data points with the label ‘start’ used the first solution as a starting point, while the ‘reuse’ approach uses the previous solution. The lower left corner corresponds with a larger focusing parameter. (middle) The model parameters when using the Cauchy norm. The focusing parameters that are used in the inverse problem are indicated with a star in the upper left plot. (bottom) The model parameters of the different regions as shown in the upper right plot. The region C is only present with the start strategy. To prevent cluttering the figure, the optimal blocky result with the reuse strategy is not plotted.

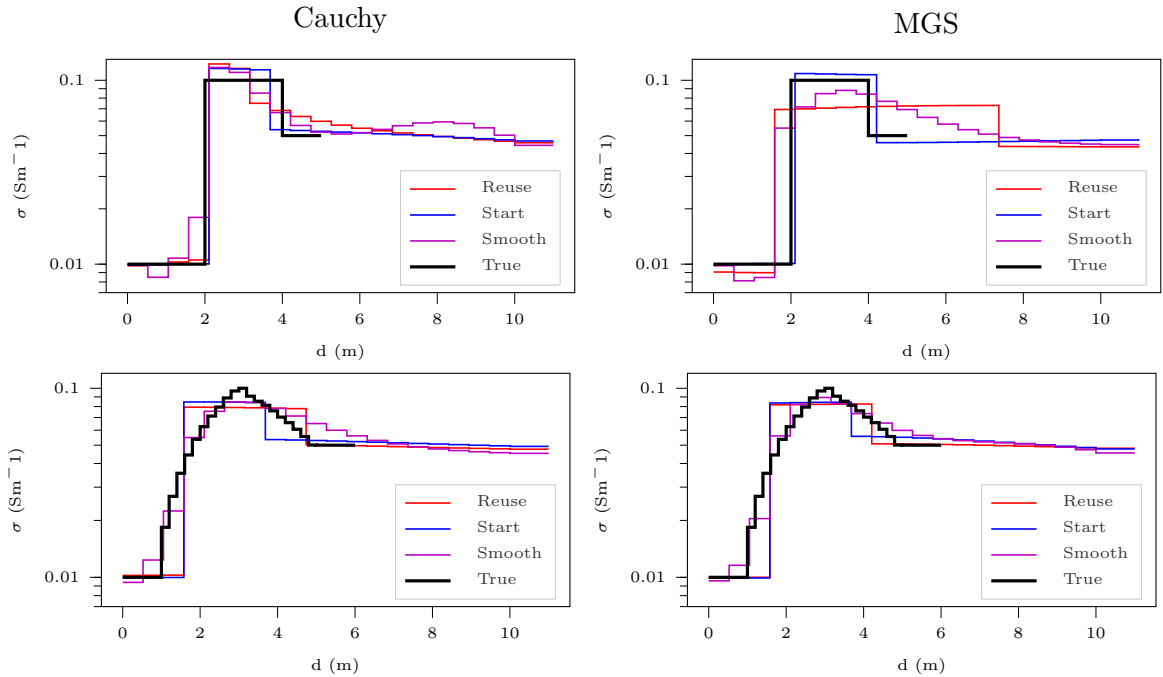


Figure 4: The model parameters for the 3-layer soil, blocky at the top and smooth at the bottom, using the Cauchy (left) and the MGS norm (right).

increase in conductivity between subsequent layers. In our gradient scheme, this is required to direct the model parameters to the minimum of the objective function. The MGS norm, however, lacks this feature, as can be seen from the horizontal line for an ever-increasing model parameter. While decreasing the focusing parameter, we shift more and more to the right of the MGS curve as plotted in Figure 1. Therefore, the gradient fails to push the model parameters to smaller values. This causes anomalies, e.g. one layer with very high or low conductivity. While the data misfit is sufficient low, we can eliminate these solutions using Occam’s razor (Constable et al., 1987).

3 Results

To illustrate the performance of our algorithm we test our method on a synthetic conductivity profile, a profile based on borehole logging and data collected at the Belgian coast.

3.1 Inversion of synthetic data

The synthetic profile depicts three layers in two versions. The first version has a clear contrast between the different layers, while the second version has a smoother transition (see Figure 4). We use a total of 19 intercoil spaces, uniformly distributed between 1 m and 19 m. At every position we measure the HCP and PRP components of the magnetic field. The dipole is at a frequency of 1.5 kHz and we put an error of 5% on the data generated with the analytical

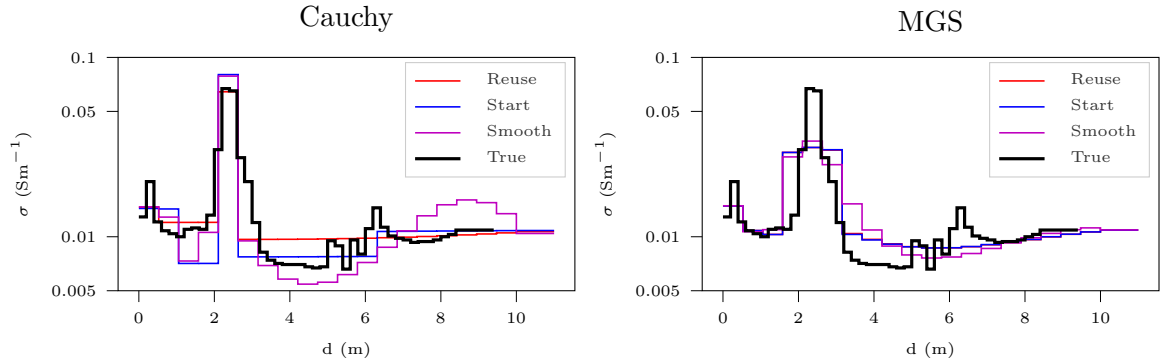


Figure 5: The model parameters with a conductivity profile based on borehole logging. Let us mention here that with the MGS norm the L -curve has the same shape using both strategies. This can also be seen in Figure 3 where the first inversions with larger values of the focusing parameter also have the same result despite the difference in strategy.

model.

The conductivity profile in our inversion has a total of 19 layers and a half-space. Since the half-space starts at a depth of 10 m, the thickness of every layer is $\frac{10}{19}$ m. We have chosen the interfaces of the true conductivity profile at 2 m and 4 m, and the inverted result can as a result never fully correspond with the true profile. Hence, we avoid the usage of any prior information, which is also the case when one is inverting real data.

In both cases and for both norms, the smooth result is able to detect the second layer but either shows some oscillations (Cauchy norm) or smears out the second layer (MGs norm). The blocky results obtained from the start strategy clearly shows the interface depths and gives a good estimate for all the electrical conductivities. While the latter remains true for the reuse strategy, the transition between layer 2 and 3 is still too smooth. Further decreasing the focusing parameter causes a clearer interface, but the data misfit increases significantly (from 1.1 tot 1.8).

As one can expect for the second version, the smooth profile captures the true profile very accurately. The blocky profiles remove the gradual transition. The position of the first interface is for all four profiles the same, while the second interface depth differs. With the reuse strategy, the depth is put at the end of the transition zone, while the start strategy places it more at the middle. Note that the data misfit for the start method together with the Cauchy norm is relatively large. While the profile looks at first sight identical to the profile of the same strategy with the MGS norm, the conductivity of the third layer is a bit different.

The second test is based on a conductivity profile obtained from borehole logging (Hermans and Irving, 2017). At this location, the soil consists of three layers. From top to bottom, we find a clay layer, then a sandy gravel one and, finally, coarser gravel. Translating this into a conductivity profile, we have a sharp peak in conductivity due to the clay layer, while below it the conductivity drops significantly due to the sandy gravel. It then slightly increases with the coarseness of the gravel.

We use the same survey setup and noise level as in the three layers case. The profiles obtained

Table 1: The data misfit for the different test cases.

	Cauchy			MGS		
	Smooth	Start	Reuse	Smooth	Start	Reuse
Blocky 3 Layers	1.06	1.10	1.09	1.16	1.17	1.66
Smooth 3 Layers	1.16	1.43	1.13	1.10	1.20	1.16
Borehole logging	1.08	1.10	1.12	1.13	1.13	1.13
Westhoek	0.89	0.93	0.98	1.02	0.90	1.19

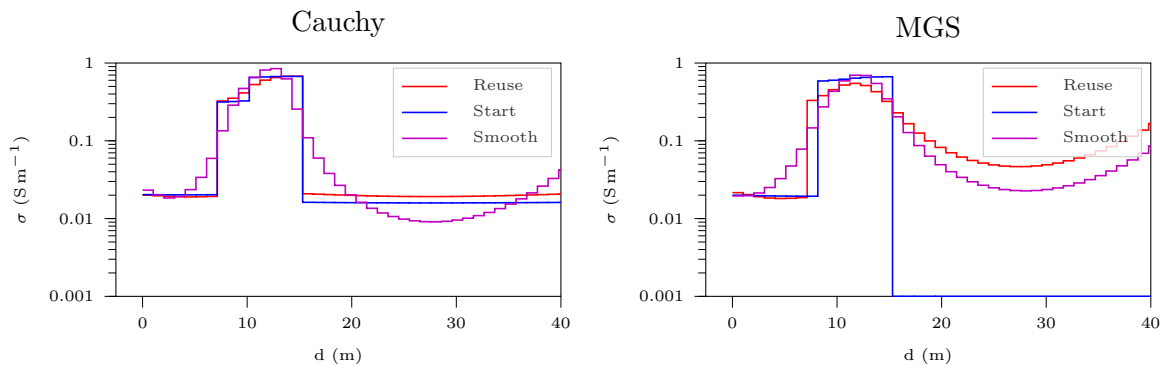


Figure 6: Inversion results for the data collected at De Westhoek nature reserve. Both norms and strategy show a sharp rise in conductivity at 5 m, in accordance with prior surveys (Vandenbohede et al., 2008; Hermans et al., 2012).

from our inversions are able to find the clay layer, see Figure 5. The MGS norm, however, underestimates the peak value of the conductivity. Furthermore, the conductivity of the sandy gravel is overestimated, causing a small transition to the coarser gravel. Note that a lower value for the focusing parameter completely removes the difference between the two lowest layers. The reuse strategy combined with the Cauchy norm also fails to get the difference between the lowest regions, but has a better value for the conductivity of the clay layer. The start strategy together with the Cauchy norm produces the best result, obtaining a good estimate for the peak value, whilst still distinguishing the two gravel layers.

The profiles obtained with the Cauchy norm are an example where the knowledge of the different strategies can be combined. All three solutions predict a thin conductive layer ($\sim \sigma = 70 \text{ mS m}^{-1}$, width = 0.5 m) starting at a depth of 2 m. Below this peak, there is a more resistive region, but the different strategies produce slightly different results. The smooth solution has some oscillations which either signals the presence of two layers with a different conductivity or are caused by the large jump in conductivity. The former is supported by the start strategy while the latter is indicated by the reuse strategy. Due to the nature of the sparse inversion, it is unlikely that a layer is introduced without a reason.

3.2 Inversion of real data

Our final case is based on data we collected at De Westhoek nature reserve, Belgium. This site is located at the Belgian coast and to promote bio-diversity, two inlets were created in the dunes (Vandenbohede et al., 2008). These inlets allowed seawater to enter an infiltration pond during high tide. While these inlets have nowadays silted up completely, there was a considerable amount of saltwater intrusion in the past. The monitoring of this intrusion is important, because tap water is pumped up from a fresh water lens in the dune aquifer.

The soil profile consists of sand on top of the Kortrijk Formation. The latter is a thick clay layer which starts roughly at 30 m depth. Below the water inlets, a semi-pervious layer, consisting mainly of clay, hinders the infiltration of the saltwater, causing a sharp peak in conductivity. Based on borehole logging and electrical resistivity tomography (ERT) surveys, the highest point of the peak starts is seen at approximately 10 m depth (at well P11), it has a width of 10 m and a height of 200 mS m^{-1} to 500 mS m^{-1} (Hermans et al., 2012). The height and width of the peak has changed in time due to the slow penetration of the seawater through the clay layer (Vandenbohede et al., 2008). The data was collected at the entrance of one of the inlets, we therefore expect that the intrusion is maximally visible.

Our data was collected using an EM34 apparatus (Geonics) (Geonics, 2018). With the EM34, measurements can be done at intercoil distances 10 m, 20 m and 40 m, at a frequency of 6.4 kHz, 1.6 kHz and 0.4 kHz respectively. Both the horizontal coplanar and vertical coplanar field can be measured. For our measurements, we assumed a data error of 5%, the measurement error according to the instruction manual.

In Figure 6, the results of our inversions are plotted. The smooth version shows, with both norms, a maximum in conductivity at 12 m with a value of 0.8 S m^{-1} . After this peak, the conductivity drops to 0.01 S m^{-1} and subsequently it increases gently. The latter may indicate the presence of the Kortrijk formation, which is just within range of our survey.

Using both norms, we clearly find a peak in conductivity of 0.3 S m^{-1} to 0.6 S m^{-1} starting and ending at 8 m and 15 m respectively. The characteristics of the peak is in accordance with the findings of previous surveys. For the Cauchy norm, both strategies obtain almost the same result with only the conductivity of the third layer being a little bit larger than if using the reuse strategy. The data misfit is therefore almost the same.

In case of the MGS norm, the results of the two strategies differ significantly. With the reuse method, a semi-smooth result is found, e.g. there is only one jump in the conductivity. The downwards slope of the conductivity spike is a gentle decrease to a value of 0.05 S m^{-1} and ends at a depth of 30 m. After reaching this low point, the conductivity increases smoothly. Contrary to the reuse strategy, the start approach shows a clear boundary for the seawater lens. While its width and height are in accordance with the results of other surveys, the conductivity of the third layer is clearly too low. The data misfit of the reuse strategy is much larger than the value of the smooth result, indicating that this result is less valid. The start method combined with the MGS norm has a similar data misfit as the Cauchy norm.

4 Conclusion

We proposed two strategies to estimate the value of the focusing parameter. In a similar way as the L -curve method, both strategies solve the inverse problem for different values of the focusing parameter and the optimal value is based on the plot of the model misfit in function of the data misfit. Both strategies start with a large value of the focusing parameter, producing a smooth result. The reuse strategy gradually lowers the value of the focusing parameter, using the previous solution as starting point for the next inverse problem. The start strategy uses the first smooth solution as starting point for every subsequent inverse problem. Both have a discontinuity in the curve, and we choose the result just after the discontinuity as the optimal result.

We tested our strategies with two ℓ_0 -norm approximating functions, i.e. MGS and Cauchy. From the synthetic cases, we can conclude that both strategies produce conductivity profiles sufficiently close to the true profile. With the data we collected at De Westhoek nature reserve, a conductivity profile is constructed which is similar to profiles obtained from earlier borehole logging and ERT surveys, see (Hermans et al., 2012).

All the data in the synthetic cases were generated with the exact 1D analytical model. Since we used the damped model as forward operator in the inversions, we can conclude that the model is adequate enough to tackle the inversion. This is further supported with the inversions where the data from our survey was used.

Future research is required to determine if our strategy is generalisable to the 2D/3D case. Due to the possible difference in constraints between the horizontal and vertical direction, i.e. a smoother lateral transition versus a blocky vertical profile, it is not straightforward to extend our strategy to two different focusing parameters. Klose et al. (2022) already used the MGS norm for a laterally constrained inversion, but used the same focusing parameter for both directions. For this case, our strategy can be easily applied as the number of parameters that need to be determined is the same as in the one dimensional case. It, however, remains to be verified if the L -curves produced with our strategies behave the same and in particular show a discontinuity in the value of the data misfit.

Acknowledgments

We are grateful to T. Hermans for useful discussions and the providing of data sets. The research leading to these results has received funding from FWO (Fund for Scientific Research, Flanders, grant 1113020N). The authors declare no conflicts of interest.

References

- R. Blaschek, A. Hördt, and A. Kemna. A new sensitivity-controlled focusing regularization scheme for the inversion of induced polarization data based on the minimum gradient support. *Geophysics*, 73(2):F45–F54, Mar. 2008. ISSN 0016-8033, 1942-2156. doi: 10.1190/1.2824820.
- S. C. Constable, R. L. Parker, and C. G. Constable. Occam’s inversion; a practical algorithm

- for generating smooth models from electromagnetic sounding data. *Geophysics*, 52(3):289–300, Mar. 1987. ISSN 0016-8033, 1942-2156. doi: 10.1190/1.1442303.
- G. P. Deidda, M. Himi, I. Barone, G. Cassiani, and A. Casas Ponsati. Frequency-Domain Electromagnetic Mapping of an Abandoned Waste Disposal Site: A Case in Sardinia (Italy). *Remote Sensing*, 14(4):878, Jan. 2022. ISSN 2072-4292. doi: 10.3390/rs14040878.
- W. Deleersnyder, B. Maveau, T. Hermans, and D. Dudal. Inversion of electromagnetic induction data using a novel wavelet-based and scale-dependent regularization term. *Geophysical Journal International*, 226(3):1715–1729, 2021. ISSN 0956-540X, 1365-246X. doi: 10.1093/gji/ggab182.
- S. Delrue, B. Maveau, and D. Dudal. A damped forward EMI model for a horizontally stratified earth. *Exploration Geophysics*, 51(4):422–433, July 2020. ISSN 0812-3985. doi: 10.1080/08123985.2019.1708717.
- C. G. Farquharson. Constructing piecewise-constant models in multidimensional minimum-structure inversions. *Geophysics*, 73(1):K1–K9, Dec. 2007. ISSN 0016-8033. doi: 10.1190/1.2816650.
- C. G. Farquharson and D. W. Oldenburg. Non-linear inversion using general measures of data misfit and model structure. *Geophysical Journal International*, 134(1):213–227, 1998. ISSN 1365-246X. doi: 10.1046/j.1365-246x.1998.00555.x.
- G. Fiandaca, J. Doetsch, G. Vignoli, and E. Auken. Generalized focusing of time-lapse changes with applications to direct current and time-domain induced polarization inversions. *Geophysical Journal International*, 203(2):1101–1112, Nov. 2015. ISSN 0956-540X. doi: 10.1093/gji/ggv350.
- Geonics. Geophysical Instrumentation for Geology, Military, Environment, Agriculture, Archaeology, and Geotechnical Studies, 2018. URL <http://www.geonics.com/html/products.html>.
- A. Guitton. Blocky regularization schemes for Full-Waveform Inversion. *Geophysical Prospecting*, 60(5):870–884, Sept. 2012. ISSN 1365-2478. doi: 10.1111/j.1365-2478.2012.01025.x.
- T. Hermans and J. Irving. Facies discrimination with electrical resistivity tomography using a probabilistic methodology: Effect of sensitivity and regularisation. *Near Surface Geophysics*, 15(1):13–25, Feb. 2017. ISSN 1569-4445. doi: 10.3997/1873-0604.2016047.
- T. Hermans, A. Vandenbohede, L. Lebbe, R. Martin, A. Kemna, J. Beaujean, and F. Nguyen. Imaging artificial salt water infiltration using electrical resistivity tomography constrained by geostatistical data. *Journal of Hydrology*, 438–439:168–180, May 2012. ISSN 0022-1694. doi: 10.1016/j.jhydrol.2012.03.021.
- T. Klose, J. Guillemoteau, G. Vignoli, and J. Tronicke. Laterally constrained inversion (LCI) of multi-configuration EMI data with tunable sharpness. *Journal of Applied Geophysics*, 196:104519, Jan. 2022. ISSN 0926-9851. doi: 10.1016/j.jappgeo.2021.104519.
- B. J. Last and K. Kubik. Compact gravity inversion. *Geophysics*, 48(6):713–721, June 1983. ISSN 0016-8033. doi: 10.1190/1.1441501.

- M. Loke, I. Acworth, and T. Dahlin. A comparison of smooth and blocky inversion methods in 2D electrical imaging surveys. *Exploration Geophysics*, 34(3):182–187, June 2003. ISSN 0812-3985. doi: 10.1071/EG03182.
- P. Martinelli and M. C. Duplaá. Laterally filtered 1D inversions of small-loop, frequency-domain EMI data from a chemical waste site. *Geophysics*, 73(4):F143–F149, July 2008. ISSN 0016-8033. doi: 10.1190/1.2917197.
- J. J. Moré and D. J. Thuente. Line Search Algorithms with Guaranteed Sufficient Decrease. *ACM Trans. Math. Softw.*, 20(3):286–307, Sept. 1994. ISSN 0098-3500. doi: 10.1145/192115.192132.
- V. Morozov. On the solution of functional equations by the method of regularization. *Dokl. Akad. Nauk SSSR*, 167(3):510–512, 1966.
- J. Nocedal and S. J. Wright. *Numerical Optimization*. Springer Series in Operations Research. Springer, New York, 2nd ed edition, 2006. ISBN 978-0-387-30303-1.
- H. Paasche and J. Tronicke. Cooperative inversion of 2D geophysical data sets: A zonal approach based on fuzzy c-means cluster analysis. *Geophysics*, 72(3):A35–A39, Mar. 2007. ISSN 0016-8033. doi: 10.1190/1.2670341.
- T. Saey, P. De Smedt, E. Meerschman, M. M. Islam, F. Meeuws, E. Van De Vijver, A. Lehouck, and M. Van Meirvenne. Electrical Conductivity Depth Modelling with a Multireceiver EMI Sensor for Prospecting Archaeological Features. *Archaeological Prospection*, 19(1):21–30, Jan. 2012. ISSN 1099-0763. doi: 10.1002/arp.425.
- E. Scudiero, R. Deiana, P. Teatini, G. Cassiani, and F. Morari. Constrained optimization of spatial sampling in salt contaminated coastal farmland using EMI and continuous simulated annealing. *Procedia Environmental Sciences*, 7:234–239, Jan. 2011. ISSN 1878-0296. doi: 10.1016/j.proenv.2011.07.041.
- R. Thibaut, T. Kremer, A. Royen, B. Kim Ngun, F. Nguyen, and T. Hermans. A new workflow to incorporate prior information in minimum gradient support (MGS) inversion of electrical resistivity and induced polarization data. *Journal of Applied Geophysics*, 187:104286, Apr. 2021. ISSN 0926-9851. doi: 10.1016/j.jappgeo.2021.104286.
- A. Tikhonov. On the stability of inverse problems. *Dokl. Akad. Nauk SSSR*, 39(5):195–198, 1943.
- A. Vandenbohede, L. Lebbe, S. Gysens, K. Delecluyse, and P. DeWolf. Salt water infiltration in two artificial sea inlets in the Belgian dune area. *Journal of Hydrology*, 360(1):77–86, Oct. 2008. ISSN 0022-1694. doi: 10.1016/j.jhydrol.2008.07.018.
- C. R. Vogel. *Computational Methods for Inverse Problems*. SIAM, Jan. 2002. ISBN 978-0-89871-550-7.
- P. Wolfe. Convergence Conditions for Ascent Methods. *SIAM Review*, 11(2):226–235, Apr. 1969. ISSN 0036-1445. doi: 10.1137/1011036.